J|A|C|S ARTICLES

Published on Web 08/19/2010

Gold Nanoframes: Very High Surface Plasmon Fields and Excellent Near-Infrared Sensors

Mahmoud A. Mahmoud and Mostafa A. El-Sayed*

Laser Dynamics Laboratory, School of Chemistry and Biochemistry, Georgia Institute of Technology, Atlanta, Georgia 30332-0400

Received May 25, 2010; E-mail: melsayed@gatech.edu

Abstract: The sensing efficiency or factor of noble metal nanoparticles is defined as the wavelength shift of the surface plasmon resonance extinction peak position per unit change in the refractive index of the surrounding medium. The sensitivity of different shapes and sizes of gold nanoparticles has been studied by many investigators and found to depend on the plasmon field strength. As a result, the sensitivity factors were found to be larger for hollow nanoparticles than for solid ones of comparable dimensions. This is due to the strong plasmonic fields resulting from the coupling between the external and internal surface plasmon fields in the hollow nanoparticles. In the present paper, the sensitivity factors of a large number of gold nanoframes of different size and wall thickness have been determined by experimental and theoretical computation (using the discrete dipole approximation method). The dependence of the sensitivity factors and the plasmon field strength on the wall thickness and the size of the nanoframes has been determined and is discussed. The sensitivity factors are found to increase linearly with the aspect ratio (wall length/wall thickness) of the nanoframes and are especially sensitive to a decrease in the wall thickness. In comparison with other plasmonic nanoparticles, it is found that nanoframes have sensitivity factors that are 12, 7, and 3 times higher than those of gold nanospheres, gold nanocubes, and gold nanorods, respectively, as well as more than several hundred units higher than those of comparable-size gold nanocages.

Introduction

Noble metal nanoparticles have attracted attention in recent decades due to their unique optical and physical properties.[1] Their unique optical properties result from localized surface plasmon resonance (SPR), which involves the coherent oscillation of the free conduction band electrons in resonance with an incident electromagnetic field.[2−5] This oscillation induces strong surface electromagnetic fields, which enhance the rate of the nanoparticles' radiative processes as well as those of neighboring electronic systems.[6−8] The rates of absorption and scattering, as well as the SPR peak position, are found to depend on the shape and size of the nanoparticles.[9,10] The SPR peak position also depends on the dielectric constant of the surrounding environment and the type of molecules bound to the surface of the nanoparticles.[11,12] A red-shift in the SPR peak position is observed as the refractive index of the surrounding medium increases.[13−15] The sensitivity of the optical properties of the plasmonic nanoparticles to the dielectric constant of the environment is the basis of their excellent sensing capabilities.[16] The sensitivity factor *S* is measured by the shift in the wavelength of the SPR peak position (in nanometers) per unit change in the refractive index (RIU) of the surrounding medium. The value of the sensitivity factor depends on the shape, size, and type of nanoparticle.[6,7] Nanoparticles with higher sensitivity factors are useful as sensors.[17,18]

The sensitivity factor of a nanoparticle is determined by the strength of the nanoparticle's plasmonic surface field. Plasmonic

(1) Kreibig, U.; Vollmer, M. *Optical Properties of Metal Clusters*; Springer Series in Materials Science *25*; Springer: Berlin, 1995.
(2) Zou, S.; Schatz, G. C. *Chem. Phys. Lett.* **2005**, *403*, 62–67.
(3) Oldenburg, S. J.; Averitt, R. D.; Westcott, S. L.; Halas, N. J. *Chem. Phys. Lett.* **1998**, *288*, 243–247.
(4) Wang, H.; Brandl, D. W.; Nordlander, P.; Halas, N. J. *Acc. Chem. Res.* **2007**, *40*, 53–62.
(5) Jain, P. K.; Huang, X.; El-Sayed, I. H.; El-Sayed, M. A. *Acc. Chem. Res.* **2008**, *41*, 1578–1586.
(6) Malinsky, M. D.; Kelly, K. L.; Schatz, G. C.; Van Duyne, R. P. *J. Phys. Chem. B* **2001**, *105*, 2343–2350.
(7) Malinsky, M. D.; Kelly, K. L.; Schatz, G. C.; Van Duyne, R. P. *J. Am. Chem. Soc.* **2001**, *123*, 1471–1482.
(8) N'Gom, M.; Li, S.; Schatz, G.; Erni, R.; Agarwal, A.; Kotov, N.; Norris, T. B. *Phys. Rev. B: Condens. Matter Mater. Phys.* **2009**, *80*, 113411/1–113411/4.
(9) Zhao, J.; Pinchuk, A. O.; McMahon, J. M.; Li, S.; Ausman, L. K.; Atkinson, A. L.; Schatz, G. C. *Acc. Chem. Res.* **2008**, *41*, 1710–1720.
(10) Sherry, L. J.; Jin, R.; Mirkin, C. A.; Schatz, G. C.; Van Duyne, R. P. *Nano Lett.* **2006**, *6*, 2060–2065.
(11) El-Sayed, I. H.; Huang, X.; El-Sayed, M. A. *Nano Lett.* **2005**, *5*, 829–834.
(12) Haes, A. J.; Zou, S.; Schatz, G. C.; Van Duyne, R. P. *J. Phys. Chem. B* **2004**, *108*, 109–116.
(13) Storhoff, J. J.; Lazarides, A. A.; Mucic, R. C.; Mirkin, C. A.; Letsinger, R. L.; Schatz, G. C. *J. Am. Chem. Soc.* **2000**, *122*, 4640–4650.
(14) Haes, A. J.; Zou, S.; Schatz, G. C.; Van Duyne, R. P. *J. Phys. Chem. B* **2004**, *108*, 6961–6968.
(15) Zhao, J.; Haes, A. J.; Zhang, X.; Zou, S.; Hicks, E. M.; Schatz, G. C.; Van Duyne, R. P. *Mater. Res. Soc. Symp. Proc.* **2006**, *900E*, 0900-O13-08.
(16) Raschke, G.; Brogl, S.; Susha, A. S.; Rogach, A. L.; Klar, T. A.; Feldmann, J.; Fieres, B.; Petkov, N.; Bein, T.; Nichtl, A.; Kuerzinger, K. *Nano Lett.* **2004**, *4*, 1853–1857.
(17) Jensen, T. R.; Duval, M. L.; Kelly, K. L.; Lazarides, A. A.; Schatz, G. C.; Van Duyne, R. P. *J. Phys. Chem. B* **1999**, *103*, 9846–9853.
(18) Mock, J. J.; Smith, D. R.; Schultz, S. *Nano Lett.* **2003**, *3*, 485–491.

10.1021/ja104532z

field coupling between nearby nanoparticles increases their plasmonic fields and thus their sensitivity factors,[19−24] which explains the enhancement of the sensitivity factors upon dimerization.[25,26]

The sensitivity factors of several nanoparticles have been reported. Solid gold nanospheres, nanocubes, and nanorods have sensitivity factors of about 40, 80, and 150−283 nm/RIU,[27] respectively. It is also found that hollow nanoparticles have enhanced sensitivity factors. For example, hollow nanospheres have a value of $S \approx 125$ nm/RIU.[16] Recently, the sensitivity of gold nanocages (hollow cubes) with a 50 nm wall length and a 4.5 nm wall thickness was found to be 408.8 nm/RIU.[28]

From the numbers reported above, hollow nanoparticles have the highest sensitivity factors. In the present paper, we focus on gold nanoframes (AuNFs), which we have previously found to have very strong plasmonic fields on account of the coupling between their interior and exterior surface fields.[29] The coupling between these two fields gives these nanoparticles additional surface fields which are expected to have greatly enhanced sensitivity factors.

The present work is aimed at determining the plasmonic fields and sensitivity factors of nanoframes of different wall lengths and thicknesses. It also attempts to develop an equation relating the value of the sensitivity factors to the geometry of the nanoframes. Since it is difficult to synthesize nanoframes of every structure we desire, we used the discrete dipole approximation (DDA) to calculate different geometries needed for the present study. The agreement between the values of the sensitivity factors measured for synthesized nanoframes and theoretically calculated gave us confidence in the DDA calculations for all other geometries.

The results are presented in four parts. Section A gives the experimental results on the sensitivity factors of a few carefully synthesized nanoframes. In section B.1, we discuss the results of the DDA theoretical simulation of the SPR spectra (which depends on the surface plasmon field) for a large selection of nanoframes of different dimensions. In section B.2, the SPR peak positions in media of different dielectric constants are calculated, from which the sensitivity factors are determined for nanoframes of different structures. In section C, a test of the DDA theoretical prediction in calculating the sensitivity factor is made by comparing its results with values observed for the synthesized nanoframes. Finally, in section D, an equation relating the sensitivity factor to the aspect ratio for the nanoframes is developed, and a comparison is made of the sensitivity factors of different plasmonic nanoparticles reported so far with those of the nanoframes.

Experimental Section

Silver nanocube (AgNC) templates are used to prepare gold nanoframes with different wall thicknesses by using the galvanic replacement technique with gold.[30] The AgNCs are prepared as follows: 35 mL of ethylene glycol (EG) is heated to 150 °C for 1 h with constant stirring. The temperature and stirring are maintained during the synthesis. Ten milliliters of EG containing 0.25 g of polyvinyl pyrrolidone (PVP) (molecular weight of ∼55 000 g) is then added, followed by the addition of 0.4 mL of sodium sulfide (3 mM) dissolved in EG. Aliquots of silver nitrate in EG (282 mM) with volumes of 3.5, 3.0, 2.0, and 1.8 mL are injected into the reaction mixture to prepare the AgNC templates with wall lengths of 80, 50, 40, and 35 nm, respectively.[31,32] The reaction is complete in 10 min after addition of the silver nitrate solution, and a nontransparent solution is formed. The AgNCs are washed by dilution with deionized (DI) water and acetone, followed by centrifugation. The resulting precipitate is then dispersed in DI water.

The AgNC templates with wall lengths of 80, 50, 40, and 35 nm are used to prepare the AuNFs with wall lengths of 83, 51, 42, and 35 nm, respectively. To prepare 83, 51, 42, and 35 nm AuNFs with wall thicknesses of 19, 10, 9, and 10 nm, respectively, the purified AgNC solutions are heated with stirring until they begin to boil. A 10 mg/L hydrogen tetrachloroaurate solution is then injected into the boiling solution slowly until the absorption spectrum of the solution shifts to 950, 1050, 1000, and 800 nm for the AuNFs, which are confirmed to have wall lengths of 83, 51, 42, and 35 nm, respectivly.[32,33] The AuNFs are cleaned by centrifugation followed by dispersion in DI water. Finally, the particles are precipitated by centrifugation, and the precipitates are transferred to chloroform solvent for use in the Langmuir−Blodgett (LB) study.

In order to determine the sensitivity of individual nanoparticles, they should be assembled at large distances of separation.[34,35] The LB technique is one of the most valuable techniques available to assemble nanoparticles into monolayers at a desired average separation.[33,36−38] In the present study, the particles are assembled at very low surface pressures to ensure that we are studying the absorption of individual particles, in order to avoid plasmon field coupling effects which affect the sensitivity measurements.[29] A Nima 611D LB trough is filled with DI water, and the surface pressure is measured with a D1L-75 pressure sensor. Nanoparticles in chloroform (1 mL) are spread over the water surface, and after 5 min, each LB film is transferred to quartz and silicon substrates using the vertical dipping method at a surface pressure of 1 mN/m. Using a Cary UV−vis−NIR apparatus (Cary 500, Version 8.01), the optical spectra of the AuNF monolayers supported on the quartz substrates are measured with the samples immersed vertically in

(19) Sih, B. C.; Wolf, M. O. *J. Phys. Chem. B* **2006**, *110*, 22298–22301.
(20) Malynych, S.; Chumanov, G. *J. Opt. A: Pure Appl. Opt.* **2006**, *8*, S144–S147.
(21) Evans, P. R.; Wurtz, G. A.; Atkinson, R.; Hendren, W.; O'Connor, D.; Dickson, W.; Pollard, R. J.; Zayats, A. V. *J. Phys. Chem. C* **2007**, *111*, 12522–12527.
(22) Rindzevicius, T.; Alaverdyan, Y.; Kaell, M.; Murray, W. A.; Barnes, W. L. *J. Phys. Chem. C* **2007**, *111*, 11806–11810.
(23) Rindzevicius, T.; Alaverdyan, Y.; Sepulveda, B.; Pakizeh, T.; Kaell, M.; Hillenbrand, R.; Aizpurua, J.; Garcia de Abajo, F. J. *J. Phys. Chem. C* **2007**, *111*, 1207–1212.
(24) Hicks, E. M.; Zou, S.; Schatz, G. C.; Spears, K. G.; Van Duyne, R. P.; Gunnarsson, L.; Rindzevicius, T.; Kasemo, B.; Kaell, M. *Nano Lett.* **2005**, *5*, 1065–1070.
(25) Jain, P. K.; El-Sayed, M. A. *Nano Lett.* **2008**, *8*, 4347–4352.
(26) Alegret, J.; Rindzevicius, T.; Pakizeh, T.; Alaverdyan, Y.; Gunnarsson, L.; Kaell, M. *J. Phys. Chem. C* **2008**, *112*, 14313–14317.
(27) Chen, H.; Kou, X.; Yang, Z.; Ni, W.; Wang, J. *Langmuir* **2008**, *24*, 5233–5237.
(28) Sun, Y.; Xia, Y. *Anal. Chem.* **2002**, *74*, 5297–5305.
(29) Mahmoud, M. A.; El-Sayed, M. A. *Nano Lett.* **2009**, *9*, 3025–3031.
(30) Chen, J.; Wiley, B.; Li, Z.-Y.; Campbell, D.; Saeki, F.; Cang, H.; Au, L.; Lee, J.; Li, X.; Xia, Y. *Adv. Mater. (Weinheim, Ger.)* **2005**, *17*, 2255–2261.
(31) Siekkinen, A. R.; McLellan, J. M.; Chen, J.; Xia, Y. *Chem. Phys. Lett.* **2006**, *432*, 491–496.
(32) Yen, C. W.; Mahmoud, M. A.; El-Sayed, M. A. *J. Phys. Chem. A* **2009**, *113*, 4340–4345.
(33) Mahmoud, M. A.; El-Sayed, M. A. *J. Phys. Chem. C* **2008**, *112*, 14618–14625.
(34) Tabor, C.; Murali, R.; Mahmoud, M.; El-Sayed, M. A. *J. Phys. Chem. A* **2009**, *113*, 1946–1953.
(35) Haes, A. J.; Zhao, J.; Zou, S.; Own, C. S.; Marks, L. D.; Schatz, G. C.; Van Duyne, R. P. *J. Phys. Chem. B* **2005**, *109*, 11158–11162.
(36) Tao, A.; Kim, F.; Hess, C.; Goldberger, J.; He, R.; Sun, Y.; Xia, Y.; Yang, P. *Nano Lett.* **2003**, *3*, 1229–1233.
(37) Tao, A.; Sinsermsuksakul, P.; Yang, P. *Angew. Chem., Int. Ed.* **2006**, *45*, 4597–4601.
(38) Mahmoud, M. A.; Tabor, C. E.; El-Sayed, M. A. *J. Phys. Chem. C* **2009**, *113*, 5493–5501.

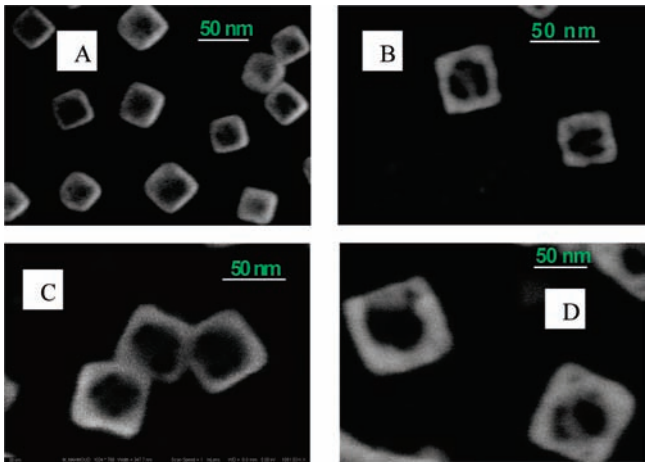

Figure 1. SEM images of AuNF with wall lengths of (A) 35, (B) 42, (C) 51, and (D) 83 nm and wall thicknesses of 10, 9, 10, and 19 nm, respectively. These images clearly show the empty structure of these nanoparticles. This is supported by the agreement of their optical spectra and those theoretically calculated.

solvents of different dielectric constants in quartz cuvettes. A clean quartz substrate immersed in each solvent is taken as a background. A Zeiss Ultra60 microscope is used to obtain the scanning electron microscopy (SEM) images of the different nanoparticles synthesized.

Results and Discussion

A. Dependence of the Sensitivity Factor on the Nanoframe Shape Factor of Synthesized Nanoframes. The spectral characteristics of the SPR of noble metals (the peak position, peak intensity, and full width at half-maximum) depend on several factors, such as the size and shape of the individual nanoparticles, the interparticle distance of the assembled particles, and the dielectric constant of the surrounding environment. In a nanosensing device,[39] the shape, size, and interparticle separation are fixed. With these parameters held constant, the shift in the SPR peak position measures the change in the dielectric constant of the nanoparticles' environment. The efficiency of the nanoparticle as a sensor is measured by the sensitivity factor (*S*), or the wavelength shift of the SPR peak per unit of reflective index change in the medium (RIU). This sensitivity factor has been studied for a variety of plasmonic nanoparticle shapes and sizes,[25,26] but little work has been done on hollow nanoparticles.[28]

In order to determine the sensitivity factors of AuNFs, four AuNFs with different dimensions are synthesized and studied. Figure 1 shows the SEM images of the four different AuNFs having wall lengths of 35, 42, 51, and 83 nm and wall thicknesses of 10, 9, 10, and 19 nm, respectively. The sensitivity factor depends on the plasmon field intensity, which is sensitive to changes in the interparticle separation and the dielectric constant of the medium. In order to study the sensitivity of the individual nanoparticles, they should be fixed at constant and large interparticle separations to prevent plasmon field coupling. The LB method is used for this purpose to reliably assemble the particles in a monolayer at a constant average separation.

The sensitivity factor was determined for various environments by measuring the SPR spectrum of different nanoparticles in a given environment. Figure 2A shows the SPR spectra of 42 nm AuNF with a wall thickness of 9 nm assembled as monolayers on the surface of a quartz substrate and measured in air, methanol, water, ethanol, tetrahydrofuran, dichloromethane, chloroform, carbon tetrachloride, and toluene. As expected, the SPR of these nanoparticles red-shifts as the refractive index of the solvent increases; this is shown in Figure 2B. The SPR spectra for the rest of the monolayers of AuNF (of wall lengths of 35, 51, and 83 nm with 10, 10, and 19 nm wall thickness, respectively) are also measured in these different solvents and are shown in Figure S1 (Supporting Information). For all nanoframes, this relationship is found to be linear, with slopes of 620 ± 15, 516 ± 24, 508 ± 33, and 409 ± 6 nm/RIU for AuNFs with wall lengths of 51, 42, 82, and 35 nm and wall thicknesses of 10, 9, 19, and 10 nm, respectively. Therefore, the ratios between the wall length (*L*) and the wall thickness (*T*), called the aspect ratio (*L*/*T*), are 5.1, 4.6, 4.3, and 3.2 for frame lengths of 51, 42, 83, and 35 nm, respectively. It is clear from Figure 2B that the sensitivity factors (the slopes of the straight lines between λ_{max} and the refractive index) increase as the aspect ratios increase.

B. Theoretical Results. 1. Calculations of Plasmonic Fields of Several Nanoframes of Different Shapes. Before we calculate the sensitivity factors, we first need to calculate the SPR spectra of nanoframes having a wide range of structures, including those of the synthesized ones discussed in the previous section (to check the theoretical prediction). SPR of a nanoparticle depends greatly on its shape and size; the SPR peak position shifts to longer wavelength as the particle size increases. The amount of scattered light also increases with increasing particle size.[6,7] Previous calculations for nanoshells[4] and hollow nanocubes[29] have shown that the optical properties are strongly dependent on the wall thickness. Our theoretical studies for AuNFs corroborate this conclusion.

In the previous section, the sensitivity factors were determined experimentally for only four nanoframes that could be carefully synthesized. In order to correlate the optical properties of the AuNFs with wall thickness for a larger selection of nanoframes, we carried out DDA calculations for AuNFs of four different wall lengths (40, 50, 80, and 90 nm), with each particle having four different wall thicknesses. The wide variation of the geometries of these 16 AuNFs allows the present work to cover a good representative population in order to study the dependence of the SPR on the wall thickness and aspect ratio. In addition, the theoretical calculations are compared with experimental results, where possible.

Figure 3A shows the SPR extinction, absorption, and scattering spectra of 50 nm wall length AuNFs with wall thicknesses of 9, 10, 11, and 12 nm. The SPR peak position is found to be centered at 916, 836, 767, and 715 nm, respectively. A red-shift in the SPR spectrum is observed as the wall thickness decreases, along with an increase in the ratio of the scattered to the absorption intensity. This calculation is extended to the other three wall lengths (40, 80, and 90 nm) and supports the first result, as shown in Figure 3B.

In order to examine the effect of the coupling between the fields on the internal frame surfaces within the cavity of the nanoframe, we used the DDA method[40,41] to calculate the field enhancement factors for the four AuNFs with wall lengths of 40, 50, 80, and 90 nm and wall thicknesses of 9.6, 12, 19.2, and 21.6 nm, respectively (Figure 4). The aspect ratio (*L*/*T*) for all of these AuNFs is 4, while the SPR peak positions are 710,

(39) Jin, R.; Wu, G.; Li, Z.; Mirkin, C. A.; Schatz, G. C. *J. Am. Chem. Soc.* **2003**, *125*, 1643–1654.
(40) Draine Bruce, T.; Flatau Piotr, J. *J. Opt. Soc. Am. A: Opt. Image Sci. Vis.* **2008**, *25*, 2693–703.
(41) Hao, E.; Li, S.; Bailey, R. C.; Zou, S.; Schatz, G. C.; Hupp, J. T. *J. Phys. Chem. B* **2004**, *108*, 1224–1229.

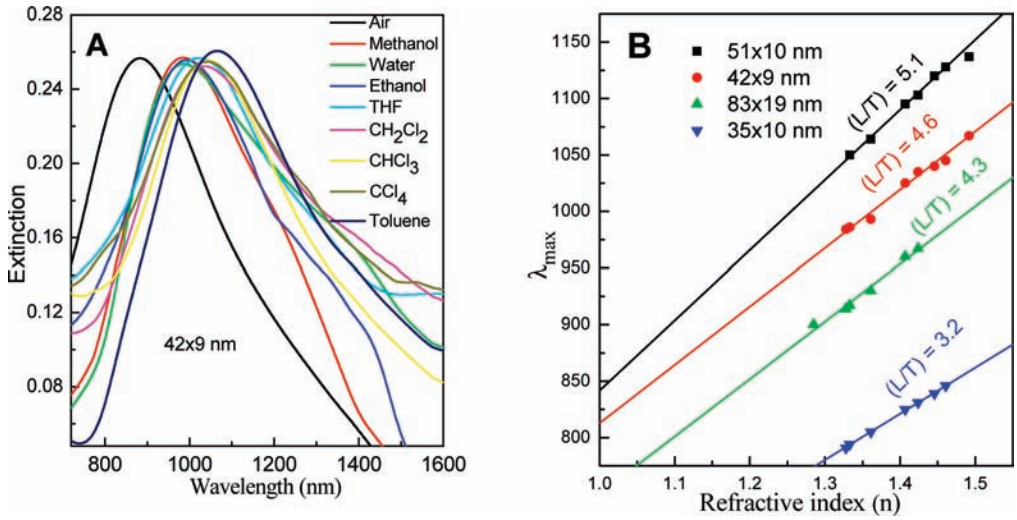

Figure 2. (A) SPR of 42 nm wall length and 9 nm wall thickness AuNF monolayers assembled on the surface of quartz substrates and measured in different solvents. (B) Relationship between the refractive index and the SPR peak maximum of AuNFs with different aspect ratios. This figure also shows that the values of the sensitivity factors (determined from the slope of each line for each aspect ratio) are 620 ± 15, 516 ± 24, 508 ± 33, and 409 ± 6 for nanoframes of aspect ratios 5.1, 4.6, 4.3, and 3.2, respectively. These sensitivity factor values are very large compared to those of other nanoparticles (see Table 2).

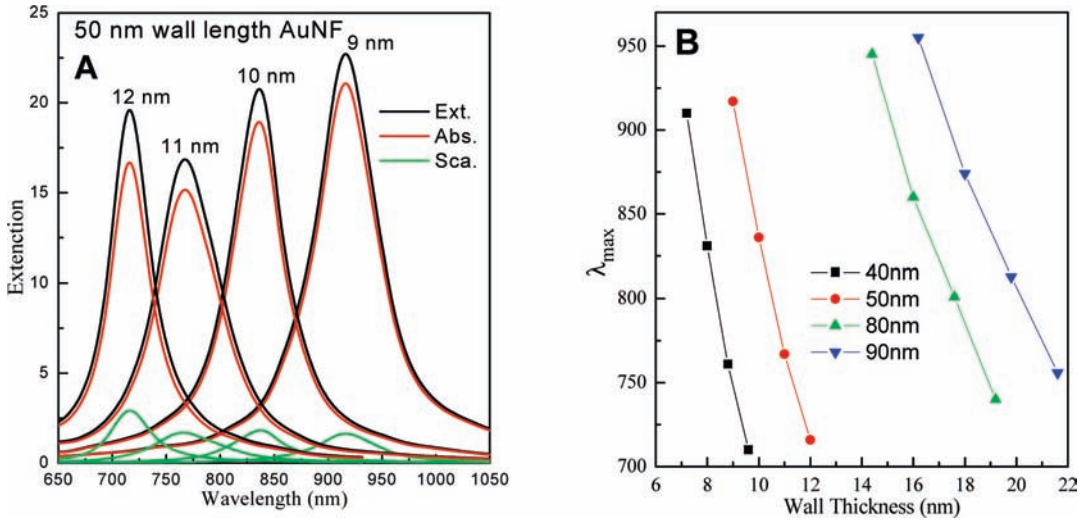

Figure 3. (A) Results of the DDA calculation of the extinction (black), absorption (red), and scattering (green) spectra of 50 nm AuNF with wall thicknesses of 9, 10, 11, and 12 nm. (B) Decrease of the SPR maximum peak position with increasing wall thickness for each studied wall length. The slopes for the two smaller particles (small length) are steeper than those for the larger particles.

716, 740, and 756 nm for the 40, 50, 80, and 90 nm particles, respectively. In contrast with the results found for other nanoparticle shapes, the plasmonic field enhancement factor of the AuNF, calculated at the wavelength of the maximum of the SPR extinction, is found to decrease as the wall length increases at a constant aspect ratio. This gives rise to the observation shown in Figure 3B. The slopes ($d\lambda/dT$) for the nanoframes of comparable sizes are similar, but the slopes for the smaller nanoframes are smaller than those for the larger nanoframes.

The data shown in Figure 3B suggest that, for nanoframes of similar L/T ratios, the magnitude of the red-shift per unit change in the wall thickness is not constant but depends on the size of the nanoframe. This suggests that as the size of the nanoframe (or the size of the cavity) decreases, the coupling between the inside and outside plasmon fields decreases. This might suggest that, in small plasmonic nanoshells, nanocages, or nanoframes, there exists a coupling between the plasmon fields of the internal surfaces which slightly decreases the strength of the coupling between the fields on the internal and external surfaces of the same frame. Since the latter coupling is the one that is dominant in determining the position of the SPR (since the thickness of the frame is smaller than the size of the cavity), the position of the SPR found for the smaller particles is not red-shifted as much as it would have been if the coupling between the internal surfaces was absent. As a result, stronger the intracavity surface coupling, the shorter is the wavelength of the SPR extinction band. This predicts that, as the intraframe distance (the nanoframe length) decreases, the wavelength of the SPR extinction band becomes shorter, as observed for the small nanoframes in Figure 4. This predicts that the field dependence of the aspect ratio (L/T) should show small deviations for small values of L due to the interaction between the fields on the internal surfaces of the cavity.

2. Calculation of the Sensitivity Factors of the Nanoframes. We studied the effect of changing the refractive index value on the SPR peak position by using 10 different solvents and a group of 16 different AuNFs (four different wall lengths having four different wall thicknesses). The SPR spectra in each solvent are calculated by the DDA method. Figure 5 shows the SPR spectra for four different AuNFs with wall lengths of 40,

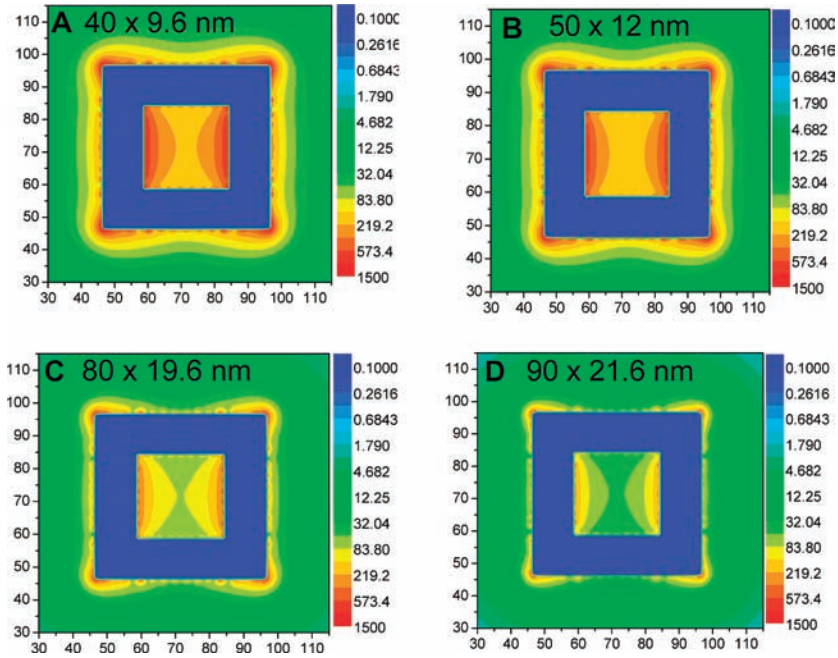

Figure 4. Field enhancement contour maps of AuNFs of the same aspect ratios ($L/T = 4.1$) with different wall lengths and wall thicknesses: (A) wall length 40 nm and 9.6 nm thickness, (B) wall length 50 nm and 12 nm thickness, (C) wall length 80 nm and 19.2 nm thickness, and (D) wall length 90 nm and 21.6 nm thickness.

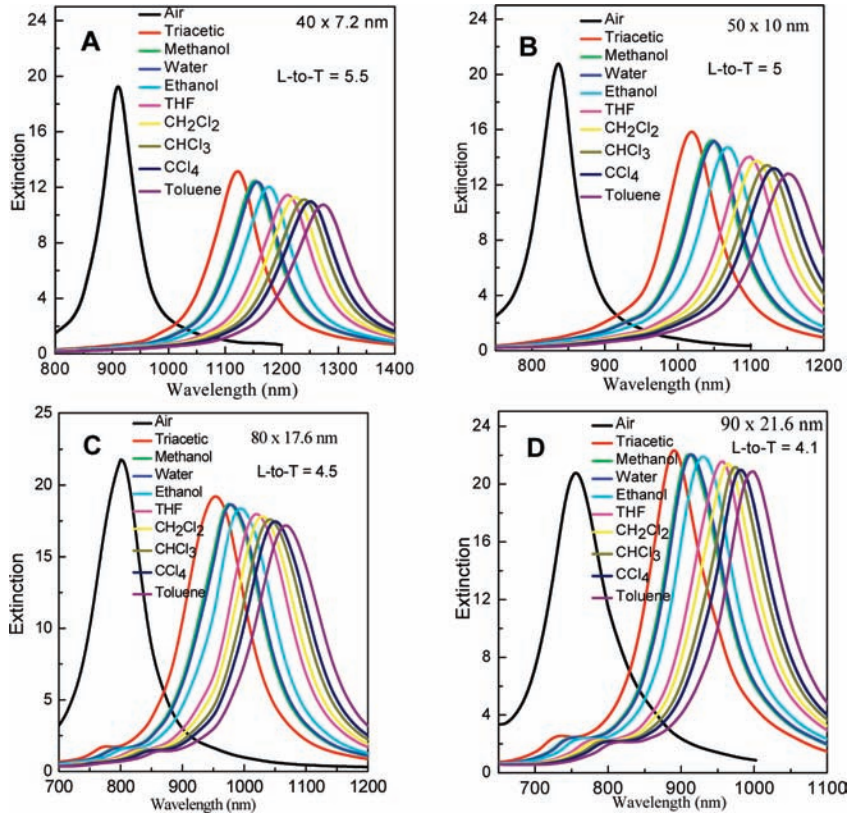

Figure 5. DDA calculation of the SPR spectra of AuNFs of different aspect ratios (L/T) simulated in different solvents: (A) wall length of 40 nm and 7.2 nm thickness (aspect ratio 5.5), (B) wall length of 50 nm and 10 nm thickness (aspect ratio 5.0), (C) wall length of 80 nm and 17.6 nm thickness (aspect ratio 4.5), and (D) wall length of 90 nm and 21.6 nm thickness (aspect ratio 4.1). Notice that as the aspect ratio increases, the wavelength of the plasmonic peaks shifts to the red.

50, 80, and 90 nm and wall thicknesses of 7.2, 10, 17.6, and 21.6 nm, respectively. The aspect ratios for that group are 5.5, 5.0, 4.5, and 4.1 for wall lengths of 40, 50, 80, and 90, respectively. The SPR spectra of these nanoframes are calculated in solvents of different dielectric constant (air, trifluoroacetic, methanol, water, ethanol, tetrahydrofuran, dichloromethane, chloroform, carbon tetrachloride, and toluene). The following conclusions can be drawn: (1) The expected red-shift of the SPR is observed as the value of the refractive index of the surrounding environment increases. (2) In any solvent, as the

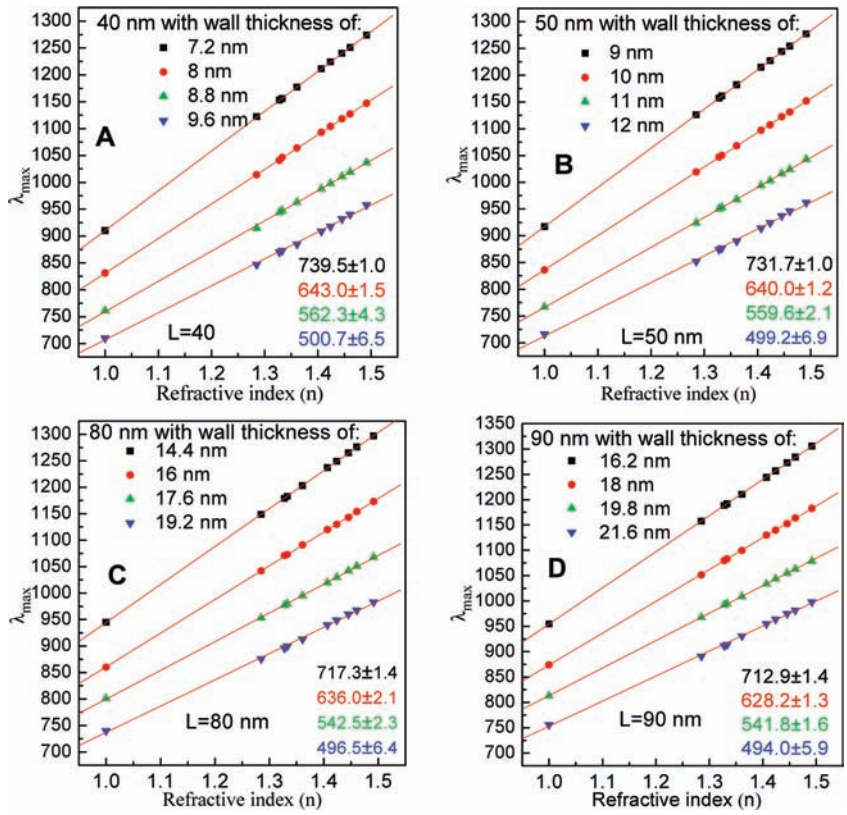

Figure 6. Relationship between the SPR peak position of AuNFs as calculated from the DDA method and the refractive indices of different surrounding solvents. The different lines in each box are for nanoframes of different aspect ratios: (top to bottom) 5.5, 5.0, 4.5, and 4.1, respectively. The different panels are for nanoframes of different wall lengths, and each line is for nanoframes of different thicknesses so as to keep the aspect ratio the same as for the corresponding lines in the other boxes: (A) 40 nm wall length but wall thicknesses of 7.2, 8, 8.8, and 9.6 nm; (B) 50 nm wall length but wall thicknesses of 9, 10, 11, and 12 nm; (C) 80 nm wall length but wall thicknesses of 14.2, 16, 17.6, and 19.2 nm; and (D) 90 nm wall length but wall thicknesses of 16.2, 18, 19.8, and 21.6 nm.

aspect ratio is increased, the SPR peak maximum shifts to longer wavelength, independent of the wall length of the nanoframe. (3) The change in the SPR peak position with changing dielectric constant of the medium increases with increasing the aspect ratio.

DDA calculations of 16 different AuNFs are carried out to determine the relationship between the refractive index of the surrounding environment and the sensitivity factor and the SPR peak position for nanoframes of different geometries. Figure 6A shows the linear relationship between the SPR peak position and the refractive index of the surrounding environment for 40 nm AuNFs with various wall thicknesses. The slope of the straight line gives the sensitivity factor (RIU) for each 40 nm AuNF. The sensitivity factor is found to increase as the nanoframe wall thickness decreases. For example, for the 40 nm AuNF, the sensitivity factor increases from 500 to 739 RIU when the wall thickness changes from 9.6 to 7.2 nm. This gives a sensitivity factor increase of 240 units for a wall thickness decrease of 2.4 nm. It should be mentioned that the decrease in the wall thickness leads to a red-shift due to the strong surface plasmon coupling between the inner and the outer surfaces of the frames. The efficiency of the nanoparticle as an optical sensor increases as the sensitivity factor increases.

Next we examined the effect of the wall length on the sensitivity factor. DDA calculations were carried out for frames with four different wall lengths and four different wall thicknesses (16 configurations). Figure 6 shows the dependence of the surface plasmon peak position on the dielectric constant of the solvents used in the calculations. The four panels in Figure 6 are for nanoframes of different wall lengths, but each panel

Table 1. Dependence of the Sensitivity Factors on the Aspect Ratio (*L*/*T*) for Nanoframes of Different Sizes As Calculated from DDA

	aspect ratio (*L*/*T*)[a]			
wall length	4.1	4.5	5.0	5.5
40	500	562	643	739
50	499	559	640	731
80	496	542	636	717
90	494	541	628	712

[a] Wall length to wall thickness.

shows the dependence of nanoframes' sensitivity factor on the wall thickness. From this figure and Table 1, it can be concluded that (1) as the wall thickness decreases the slope of λ vs dielectric constant (i.e., the sensitivity factor) increases and (2) the slopes (i.e., the sensitivity factors) of particles of similar aspect ratios but different lengths shown in the four different panels in Figure 6 seem to be similar. This suggests that the sensitivity factors, like the surface plasmon field strength (which is determined dominantly by the coupling of the inner and outer surface plasmon fields), depend on the separation of the inner and outer surface plasmon fields, which is a function of wall thickness and not very much of wall length, if the aspect ratios are comparable.

From Figure 6 and Table 1, the following can be concluded: (1) The sensitivity factors are strongly correlated with the aspect ratio of the nanoframes with a small dependence on the nanoframe size. The sensitivity factor changes from ~500 to 720 nm/RIU for a change in the aspect ratio from 4 to 5.5 for the same wall length. (2) Smaller nanoframes have slightly larger

Table 2. Comparison of the Experimentally Determined Sensitivity Factors *S* for Different Plasmonic Nanoparticle Structures

particle shape		*S* (nm/RIU)
gold nanospheres		44[27]
gold nanocubes		83[27]
gold nanorods		150−285[27]
hexagonal silver array		191[42]
hollow gold nanospheres		125[16]
gold nanocages	50 nm wall length, 5 nm thickness	408[28]
gold nanoframes	51 nm wall length, 10 nm thickness	620 ± 15
	42 nm wall length, 9 nm thickness	516 ± 24
	83 nm wall length, 19 nm thickness	508 ± 33
	35 nm wall length, 10 nm thickness	409 ± 6

sensitivity factors than larger ones. (3) The effect of changing the wall thickness on the sensitivity factors is larger for small nanoframes than for larger ones. For nanoframes with wall lengths of 40, 50, 80, and 90 nm, the sensitivity factors are 100, 77, 46, and 40 nm/RIU, respectively. (4) From the above, one can conclude that small nanoframes with thin walls are the most sensitive nanoparticles.

C. Comparison of the Experimental Results with the DDA Calculations. In order to test the accuracy of DDA in calculating the sensitivity factors, we compared the experimentally determined values for the synthesized nanoframes with the DDA results of the AuNFs of the same structures. The experimentally determined sensitivity factors were 620 ± 15, 516 ± 24, and 508 ± 33 nm/RIU for AuNFs with wall lengths of 51, 42, and 82 and wall thicknesses of 10, 9, and 19 nm, respectively. These results should be compared with the calculated values for the AuNFs with wall lengths of 50, 40, and 80 nm and wall thicknesses of 10, 8.8, and 19.2 nm, respectively: the calculated sensitivity factors are 640 ± 1.2, 562 ± 4.3, and 498 ± 6.4 nm/RIU. It is clear that the agreement is very good indeed and is within experimental error.

D. Comparison of the Sensitivity Factors of Different Plasmonic Nanoparticles. Finally, we compared the sensitivity factors of the nanoframes determined in the present work with those determined previously by others for solid and hollow nanoparticles of different shapes. This is shown in Table 2. From the table it is clear that the nanoframes have the highest sensitivity factors. Only the nanocage has a value that is close to that of the nanoframe. However, the studied nanocage has a much thicker wall. Since the sensitivity factor is very sensitive to the wall thickness, we need to compare nanocages and nanoframes having the same wall lengths and especially the same wall thicknesses. Thus, an equation that relates the change of the refractive index with the change of the wall thickness of the nanoframe is needed.

The aspect ratio is reasonably correlated with the sensitivity factor *S*. Therefore, by fitting all the experimental and theoretical results for the sensitivity factors vs the aspect ratio, we obtained eq 1 for nanoframes having L/T in the range of 4−5.5.

$$S = \Delta\lambda_{max}/\Delta n = 164(L/T) - 180 \quad (1)$$

where λ_{max} is the SPR position (wavelength band maximum, in nm) and n is the refractive index of the medium (RIU). From Table 2, a nanocage with a 50 nm wall length and 5 nm wall thickness has a sensitivity factor of 408 nm/RIU. The nanoframe with a 51 nm wall length and 10 nm wall thickness has a sensitivity factor of 620 nm/RIU. If we decrease the wall thickness of the 50 nm nanoframe by 5 nm and use eq 1, the expected sensitivity factor is 1460 nm/RIU. This predicts that the sensitivity factor of a nanoframe is 3 times larger than that of a nanocage with comparable dimensions. Of course, one should be careful, as we do not know the exact geometry of the nanocage, its size, and the effect of the holes in its walls.

The reason for the greatly enhanced plasmonic fields and sensitivity factors of nanoframes over those of nanocages is not yet known. A possible reason could be the much more focused plasmonic fields along the narrow frames and their sharp corners compared to the diffuse field on the larger surface area of the nanocage walls. This is analogous to the known larger plasmonic fields on the tip of prismatic nanoparticles than that on the surface of a disk- or spherical-shaped nanoparticle.

Conclusions

In this study, we have used synthetic and DDA theoretical computation methods to evaluate the plasmonic fields and the sensitivity factors of a large number of gold nanoframes of different structures. Table 1 and eq 1 give the dependence of the sensitivity factors on the aspect ratio of the nanoframes examined. Table 2 compares the sensitivity factors of the AuNFs examined in this study with those for other previously reported shapes.[16,27,42] The sensitivity factors of hollow nanoparticles are larger than those of solid nanoparticles of similar dimensions. This is a reflection of the fact that hollow nanoparticles have stronger surface plasmonic fields, resulting from the coupling between the surface plasmon fields on the exterior and interior walls. For small nanoframes (small wall lengths), the coupling between the inner surface fields within the nanoparticles becomes non-negligible and affects the observed values of the SPR wavelength. The sensitivity factor of nanoframes is strongly and linearly dependent on the aspect ratio (L/T, see eq 1) and is much higher for nanoframes of small size with large aspect ratios. Nanoframes have the strongest plasmonic fields and largest sensitivity factors of any single nanoparticles known. They are excellent nanosensors in the near-infrared region.

Acknowledgment. This work was supported by the Division of Materials Research of the National Science Foundation (No. 0906822). We thank F. Saira for proofreading the manuscript.

Supporting Information Available: SPR spectra of gold nanoframes having different wall lengths and wall thicknesses in different solvents, including measured experimental results and DDA simulation. This material is available free of charge via the Internet at http://pubs.acs.org.

JA104532Z

(42) Khalavka, Y.; Becker, J.; Soennichsen, C. *J. Am. Chem. Soc.* **2009**, *131*, 1871–1875.